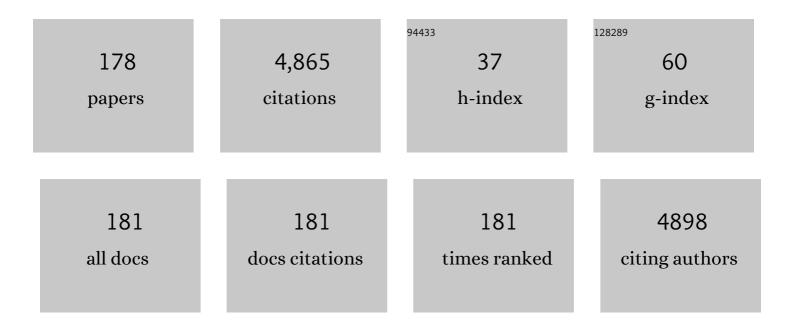
Dimitrios C Karampinos

List of Publications by Year in descending order

Source: https://exaly.com/author-pdf/9537594/publications.pdf Version: 2024-02-01



#	Article	IF	CITATIONS
1	Bone marrow fat composition as a novel imaging biomarker in postmenopausal women with prevalent fragility fractures. Journal of Bone and Mineral Research, 2013, 28, 1721-1728.	2.8	272
2	Does vertebral bone marrow fat content correlate with abdominal adipose tissue, lumbar spine bone mineral density, and blood biomarkers in women with type 2 diabetes mellitus?. Journal of Magnetic Resonance Imaging, 2012, 35, 117-124.	3.4	196
3	Quantitative MRI and spectroscopy of bone marrow. Journal of Magnetic Resonance Imaging, 2018, 47, 332-353.	3.4	185
4	Cartilage and meniscal T2 relaxation time as non-invasive biomarker for knee osteoarthritis and cartilage repair procedures. Osteoarthritis and Cartilage, 2013, 21, 1474-1484.	1.3	159
5	Neural activation of swallowing and swallowingâ€related tasks in healthy young adults: An attempt to separate the components of deglutition. Human Brain Mapping, 2009, 30, 3209-3226.	3.6	142
6	Bone marrow fat quantification in the presence of trabecular bone: Initial comparison between waterâ€fat imaging and singleâ€voxel MRS. Magnetic Resonance in Medicine, 2014, 71, 1158-1165.	3.0	127
7	Quadriceps intramuscular fat fraction rather than muscle size is associated with knee osteoarthritis. Osteoarthritis and Cartilage, 2014, 22, 226-234.	1.3	108
8	Non-invasive Measurement of Brown Fat Metabolism Based on Optoacoustic Imaging of Hemoglobin Gradients. Cell Metabolism, 2018, 27, 689-701.e4.	16.2	105
9	Characterization of the regional distribution of skeletal muscle adipose tissue in type 2 diabetes using chemical shiftâ€based water/fat separation. Journal of Magnetic Resonance Imaging, 2012, 35, 899-907.	3.4	103
10	<i>T</i> ₁ â€corrected fat quantification using chemical shiftâ€based water/fat separation: Application to skeletal muscle. Magnetic Resonance in Medicine, 2011, 66, 1312-1326.	3.0	102
11	Quantitative assessment of fat infiltration in the rotator cuff muscles using water-fat MRI. Journal of Magnetic Resonance Imaging, 2014, 39, 1178-1185.	3.4	88
12	Assessment of whole spine vertebral bone marrow fat using chemical shiftâ€encoding based waterâ€fat MRI. Journal of Magnetic Resonance Imaging, 2015, 42, 1018-1023.	3.4	82
13	The Effects of a Higher Protein Intake During Energy Restriction on Changes in Body Composition and Physical Function in Older Women. Journals of Gerontology - Series A Biological Sciences and Medical Sciences, 2011, 66A, 1218-1225.	3.6	81
14	MR-Based Assessment of Bone Marrow Fat in Osteoporosis, Diabetes, and Obesity. Frontiers in Endocrinology, 2016, 7, 74.	3.5	70
15	MR-based assessment of body fat distribution and characteristics. European Journal of Radiology, 2016, 85, 1512-1518.	2.6	68
16	Association of paraspinal muscle water–fat MRI-based measurements with isometric strength measurements. European Radiology, 2019, 29, 599-608.	4.5	66
17	Validation of bone marrow fat quantification in the presence of trabecular bone using MRI. Journal of Magnetic Resonance Imaging, 2015, 42, 539-544.	3.4	65
18	Anatomical Variation of Age-Related Changes in Vertebral Bone Marrow Composition Using Chemical Shift Encoding-Based Water–Fat Magnetic Resonance Imaging. Frontiers in Endocrinology, 2018, 9, 141.	3.5	65

#	Article	IF	CITATIONS
19	Intravoxel partially coherent motion technique: Characterization of the anisotropy of skeletal muscle microvasculature. Journal of Magnetic Resonance Imaging, 2010, 31, 942-953.	3.4	62
20	<scp>MRI</scp> â€Based Quantitative Osteoporosis Imaging at the Spine and Femur. Journal of Magnetic Resonance Imaging, 2021, 54, 12-35.	3.4	61
21	Comparison of clinical semi-quantitative assessment of muscle fat infiltration with quantitative assessment using chemical shift-based water/fat separation in MR studies of the calf of post-menopausal women. European Radiology, 2012, 22, 1592-1600.	4.5	58
22	Removal of olefinic fat chemical shift artifact in diffusion MRI. Magnetic Resonance in Medicine, 2011, 65, 692-701.	3.0	57
23	Reporting Guidelines, Review of Methodological Standards, and Challenges Toward Harmonization in Bone Marrow Adiposity Research. Report of the Methodologies Working Group of the International Bone Marrow Adiposity Society. Frontiers in Endocrinology, 2020, 11, 65.	3.5	53
24	The need for <i>T</i> ₂ correction on MRS-based vertebral bone marrow fat quantification: implications for bone marrow fat fraction age dependence. NMR in Biomedicine, 2015, 28, 432-439.	2.8	52
25	MRâ€detected changes in liver fat, abdominal fat, and vertebral bone marrow fat after a fourâ€week calorie restriction in obese women. Journal of Magnetic Resonance Imaging, 2015, 42, 1272-1280.	3.4	51
26	Correction of phase errors in quantitative water–fat imaging using a monopolar timeâ€interleaved multiâ€echo gradient echo sequence. Magnetic Resonance in Medicine, 2017, 78, 984-996.	3.0	50
27	Multiâ€center evaluation of stability and reproducibility of quantitative MRI measures in healthy calf muscles. NMR in Biomedicine, 2019, 32, e4119.	2.8	50
28	Reduced somatosensory activations in swallowing with age. Human Brain Mapping, 2011, 32, 730-743.	3.6	48
29	Age-Related Differences in Laterality of Cortical Activations in Swallowing. Dysphagia, 2010, 25, 238-249.	1.8	47
30	Cartilage Repair Surgery: Outcome Evaluation by Using Noninvasive Cartilage Biomarkers Based on Quantitative MRI Techniques?. BioMed Research International, 2014, 2014, 1-17.	1.9	46
31	Modeling of <i>T</i> ₂ * decay in vertebral bone marrow fat quantification. NMR in Biomedicine, 2015, 28, 1535-1542.	2.8	46
32	Measurement of vertebral bone marrow proton density fat fraction in children using quantitative water–fat MRI. Magnetic Resonance Materials in Physics, Biology, and Medicine, 2017, 30, 449-460.	2.0	46
33	Exploration of New Contrasts, Targets, and MR Imaging and Spectroscopy Techniques for Neuromuscular Disease – A Workshop Report of Working Group 3 of the Biomedicine and Molecular Biosciences COST Action BM1304 MYO-MRI. Journal of Neuromuscular Diseases, 2019, 6, 1-30.	2.6	46
34	Discrimination Between Brown and White Adipose Tissue Using a 2-Point Dixon Water–Fat Separation Method in Simultaneous PET/MRI. Journal of Nuclear Medicine, 2015, 56, 1742-1747.	5.0	45
35	Myofiber Ellipticity as an Explanation for Transverse Asymmetry of Skeletal Muscle Diffusion MRI In Vivo Signal. Annals of Biomedical Engineering, 2009, 37, 2532-2546.	2.5	43
36	Reduction of the n–6:n–3 long-chain PUFA ratio during pregnancy and lactation on offspring body composition: follow-up results from a randomized controlled trial up to 5 y of age. American Journal of Clinical Nutrition, 2016, 103, 1472-1481.	4.7	41

#	Article	IF	CITATIONS
37	MRI biomarkers of proximal nerve injury in CIDP. Annals of Clinical and Translational Neurology, 2018, 5, 19-28.	3.7	40
38	Automated unsupervised multiâ€parametric classification of adipose tissue depots in skeletal muscle. Journal of Magnetic Resonance Imaging, 2013, 37, 917-927.	3.4	39
39	Associations Between Lumbar Vertebral Bone Marrow and Paraspinal Muscle Fat Compositions—An Investigation by Chemical Shift Encoding-Based Water-Fat MRI. Frontiers in Endocrinology, 2018, 9, 563.	3.5	39
40	Association of MRS-Based Vertebral Bone Marrow Fat Fraction with Bone Strength in a Human In Vitro Model. Journal of Osteoporosis, 2015, 2015, 1-8.	0.5	36
41	Highâ€resolution diffusion tensor imaging of the human pons with a reduced fieldâ€ofâ€view, multishot, variableâ€density, spiral acquisition at 3 T. Magnetic Resonance in Medicine, 2009, 62, 1007-1016.	3.0	35
42	Magnetic Resonance Imaging Techniques for Brown Adipose Tissue Detection. Frontiers in Endocrinology, 2020, 11, 421.	3.5	35
43	CT-like images based on T1 spoiled gradient-echo and ultra-short echo time MRI sequences for the assessment of vertebral fractures and degenerative bone changes of the spine. European Radiology, 2021, 31, 4680-4689.	4.5	35
44	Double Inversion Recovery Sequence of the Cervical Spinal Cord in Multiple Sclerosis and Related Inflammatory Diseases. American Journal of Neuroradiology, 2015, 36, 219-225.	2.4	34
45	Automatic segmentation of abdominal organs and adipose tissue compartments in water-fat MRI: Application to weight-loss in obesity. European Journal of Radiology, 2016, 85, 1613-1621.	2.6	34
46	Association of proton density fat fraction in adipose tissue with imaging-based and anthropometric obesity markers in adults. International Journal of Obesity, 2018, 42, 175-182.	3.4	34
47	Association of Quadriceps Muscle Fat With Isometric Strength Measurements in Healthy Males Using Chemical Shift Encoding-Based Water-Fat Magnetic Resonance Imaging. Journal of Computer Assisted Tomography, 2016, 40, 447-451.	0.9	32
48	Considerations in highâ€resolution skeletal muscle diffusion tensor imaging using singleâ€shot echo planar imaging with stimulatedâ€echo preparation and sensitivity encoding. NMR in Biomedicine, 2012, 25, 766-778.	2.8	31
49	Chemical shiftâ€based water/fat separation in the presence of susceptibilityâ€induced fat resonance shift. Magnetic Resonance in Medicine, 2012, 68, 1495-1505.	3.0	30
50	Texture analysis of vertebral bone marrow using chemical shift encoding–based water-fat MRI: a feasibility study. Osteoporosis International, 2019, 30, 1265-1274.	3.1	30
51	Accelerating anatomical 2D turbo spin echo imaging of the ankle using compressed sensing. European Journal of Radiology, 2019, 118, 277-284.	2.6	28
52	Associations of thigh muscle fat infiltration with isometric strength measurements based on chemical shift encoding-based water-fat magnetic resonance imaging. European Radiology Experimental, 2019, 3, 45.	3.4	27
53	Current trends and challenges in MRI acquisitions to investigate brain function. International Journal of Psychophysiology, 2009, 73, 33-42.	1.0	26
54	Diffusion tensor imaging and <i>T</i> ₂ relaxometry of bilateral lumbar nerve roots: feasibility of inâ€plane imaging. NMR in Biomedicine, 2013, 26, 630-637.	2.8	26

#	Article	IF	CITATIONS
55	Improving chemical shift encodingâ€based water–fat separation based on a detailed consideration of magnetic field contributions. Magnetic Resonance in Medicine, 2018, 80, 990-1004.	3.0	26
56	A novel approach for modelling LiBr–H2O falling film absorption on cooled horizontal bundle of tubes. International Journal of Refrigeration, 2012, 35, 1115-1122.	3.4	25
57	Five-Year Outcomes After Treatment for Acute Instability of the Tibiofibular Syndesmosis Using a Suture-Button Fixation System. Orthopaedic Journal of Sports Medicine, 2017, 5, 232596711770285.	1.7	25
58	Improved Brachial Plexus Visualization Using an Adiabatic iMSDE-Prepared STIR 3D TSE. Clinical Neuroradiology, 2019, 29, 631-638.	1.9	25
59	MRI of the inferior alveolar nerve and lingual nerve—anatomical variation and morphometric benchmark values of nerve diameters in healthy subjects. Clinical Oral Investigations, 2020, 24, 2625-2634.	3.0	25
60	Magnetic resonance cholangiopancreatography at 3 Tesla: Image quality comparison between 3D compressed sensing and 2D single-shot acquisitions. European Journal of Radiology, 2019, 115, 53-58.	2.6	24
61	Magnetic resonance imaging of obesity and metabolic disorders: Summary from the 2019 ISMRM Workshop. Magnetic Resonance in Medicine, 2020, 83, 1565-1576.	3.0	24
62	Diffusionâ€weighted stimulated echo acquisition mode (DWâ€STEAM) MR spectroscopy to measure fat unsaturation in regions with low protonâ€density fat fraction. Magnetic Resonance in Medicine, 2016, 75, 32-41.	3.0	23
63	Quantitative magnetic resonance imaging of the upper trapezius muscles – assessment of myofascial trigger points in patients with migraine. Journal of Headache and Pain, 2019, 20, 8.	6.0	23
64	Differentiating supraclavicular from gluteal adipose tissue based on simultaneous PDFF and T ₂ * mapping using a 20â€echo gradientâ€echo acquisition. Journal of Magnetic Resonance Imaging, 2019, 50, 424-434.	3.4	23
65	Magnetic resonance imaging as a diagnostic tool for periodontal disease: A prospective study with correlation to standard clinical findings—Is there added value?. Journal of Clinical Periodontology, 2021, 48, 929-948.	4.9	23
66	High-Resolution Bone Imaging for Osteoporosis Diagnostics and Therapy Monitoring Using Clinical MDCT and MRI. Current Medicinal Chemistry, 2013, 20, 4844-4852.	2.4	23
67	Two patients with G <i>MPPB</i> mutation: The overlapping phenotypes of limb-girdle myasthenic syndrome and limb-girdle muscular dystrophy dystroglycanopathy. Muscle and Nerve, 2017, 56, 334-340.	2.2	22
68	Thigh muscle segmentation of chemical shift encoding-based water-fat magnetic resonance images: The reference database MyoSegmenTUM. PLoS ONE, 2018, 13, e0198200.	2.5	22
69	Paraspinal Muscle DTI Metrics Predict Muscle Strength. Journal of Magnetic Resonance Imaging, 2019, 50, 816-823.	3.4	22
70	Gender- and Age-Related Changes in Trunk Muscle Composition Using Chemical Shift Encoding-Based Water–Fat MRI. Nutrients, 2018, 10, 1972.	4.1	21
71	Techniques and Applications of Magnetic Resonance Imaging for Studying Brown Adipose Tissue Morphometry and Function. Handbook of Experimental Pharmacology, 2018, 251, 299-324.	1.8	20
72	Decreased water T ₂ in fatty infiltrated skeletal muscles of patients with neuromuscular diseases. NMR in Biomedicine, 2019, 32, e4111.	2.8	20

#	Article	IF	CITATIONS
73	On the sensitivity of quantitative susceptibility mapping for measuring trabecular bone density. Magnetic Resonance in Medicine, 2019, 81, 1739-1754.	3.0	20
74	Magnetic resonance imaging based <scp>computerâ€guided</scp> dental implant surgery—A clinical pilot study. Clinical Implant Dentistry and Related Research, 2020, 22, 612-621.	3.7	20
75	B1-insensitive T2 mapping of healthy thigh muscles using a T2-prepared 3D TSE sequence. PLoS ONE, 2017, 12, e0171337.	2.5	18
76	Deep learning–based acceleration of Compressed Sense MR imaging of the ankle. European Radiology, 2022, 32, 8376-8385.	4.5	18
77	A realistic approach to model LiBr–H2O smooth falling film absorption on a vertical tube. Applied Thermal Engineering, 2003, 23, 2269-2283.	6.0	17
78	Ex vivo porcine model to measure pH dependence of chemical exchange saturation transfer effect of glycosaminoglycan in the intervertebral disc. Magnetic Resonance in Medicine, 2014, 71, 1743-1749.	3.0	17
79	ADC Quantification of the Vertebral Bone Marrow Water Component: Removing the Confounding Effect of Residual Fat. Magnetic Resonance in Medicine, 2017, 78, 1432-1441.	3.0	17
80	<i>T</i> ₂ mapping with magnetizationâ€prepared 3D TSE based on a modified BIRâ€4Â <i>T</i> ₂ preparation. NMR in Biomedicine, 2017, 30, e3773.	2.8	17
81	T2-relaxation time of cartilage repair tissue is associated with bone remodeling after spongiosa-augmented matrix-associated autologous chondrocyte implantation. Osteoarthritis and Cartilage, 2019, 27, 90-98.	1.3	17
82	Quantitative 3-T Magnetic Resonance Imaging After Matrix-Associated Autologous Chondrocyte Implantation With Autologous Bone Grafting of the Knee: The Importance of Subchondral Bone Parameters. American Journal of Sports Medicine, 2021, 49, 476-486.	4.2	17
83	\${K}\$-Space and Image-Space Combination for Motion-Induced Phase-Error Correction in Self-Navigated Multicoil Multishot DWI. IEEE Transactions on Medical Imaging, 2009, 28, 1770-1780.	8.9	16
84	Imaging of the lumbar plexus: Optimized refocusing flip angle train design for 3D TSE. Journal of Magnetic Resonance Imaging, 2016, 43, 789-799.	3.4	16
85	Orthogonally combined motion―and diffusionâ€sensitized driven equilibrium (OCâ€MDSDE) preparation for vessel signal suppression in 3D turbo spin echo imaging of peripheral nerves in the extremities. Magnetic Resonance in Medicine, 2018, 79, 407-415.	3.0	16
86	Improved body quantitative susceptibility mapping by using a variableâ€layer singleâ€minâ€cut graphâ€cut for fieldâ€mapping. Magnetic Resonance in Medicine, 2021, 85, 1697-1712.	3.0	16
87	A distribution-centered approach for analyzing human adipocyte size estimates and their association with obesity-related traits and mitochondrial function. International Journal of Obesity, 2021, 45, 2108-2117.	3.4	16
88	Transcriptome and fatty-acid signatures of adipocyte hypertrophy and its non-invasive MR-based characterization in human adipose tissue. EBioMedicine, 2022, 79, 104020.	6.1	16
89	In Vivo Study of Cross-Sectional Skeletal Muscle Fiber Asymmetry with Diffusion-Weighted MRI. Annual International Conference of the IEEE Engineering in Medicine and Biology Society, 2007, 2007, 327-30.	0.5	15
90	Analysis of phase error effects in multishot diffusion-prepared turbo spin echo imaging. Quantitative Imaging in Medicine and Surgery, 2017, 7, 238-250.	2.0	15

#	Article	IF	CITATIONS
91	Comparison of regional bone marrow adiposity characteristics at the hip of underweight and weight-recovered women with anorexia nervosa using magnetic resonance spectroscopy. Bone, 2019, 127, 135-145.	2.9	15
92	Measuring large lipid droplet sizes by probing restricted lipid diffusion effects with diffusionâ€weighted MRS at 3T. Magnetic Resonance in Medicine, 2019, 81, 3427-3439.	3.0	15
93	High Isotropic Resolution T2 Mapping of the Lumbosacral Plexus with T2-Prepared 3D Turbo Spin Echo. Clinical Neuroradiology, 2019, 29, 223-230.	1.9	15
94	Vertebral bone marrow T2* mapping using chemical shift encoding-based water-fat separation in the quantitative analysis of lumbar osteoporosis and osteoporotic fractures. Quantitative Imaging in Medicine and Surgery, 2021, 11, 3715-3725.	2.0	15
95	Generalized parameter estimation in multi-echo gradient-echo-based chemical species separation. Quantitative Imaging in Medicine and Surgery, 2020, 10, 554-567.	2.0	15
96	A detailed analysis of water-vapour absorption in LiBr–H2O solution on a cooled horizontal tube. Applied Thermal Engineering, 2006, 26, 2095-2102.	6.0	14
97	Generation of an atlas of the proximal femur and its application to trabecular bone analysis. Magnetic Resonance in Medicine, 2011, 66, 1181-1191.	3.0	14
98	Vertebral Bone Marrow Heterogeneity Using Texture Analysis of Chemical Shift Encoding-Based MRI: Variations in Age, Sex, and Anatomical Location. Frontiers in Endocrinology, 2020, 11, 555931.	3.5	14
99	Imaging modalities for diagnosis and monitoring of cancer cachexia. EJNMMI Research, 2021, 11, 94.	2.5	14
100	Isotropic resolution diffusion tensor imaging of lumbosacral and sciatic nerves using a phaseâ€corrected diffusionâ€prepared 3D turbo spin echo. Magnetic Resonance in Medicine, 2018, 80, 609-618.	3.0	13
101	Water T 2 Mapping in Fatty Infiltrated Thigh Muscles of Patients With Neuromuscular Diseases Using a T 2 â€Prepared 3D Turbo Spin Echo With SPAIR. Journal of Magnetic Resonance Imaging, 2020, 51, 1727-1736.	3.4	13
102	T2-Weighted Dixon Turbo Spin Echo for Accelerated Simultaneous Grading of Whole-Body Skeletal Muscle Fat Infiltration and Edema in Patients With Neuromuscular Diseases. Journal of Computer Assisted Tomography, 2018, 42, 574-579.	0.9	12
103	Acceleration of chemical shift encoding-based water fat MRI for liver proton density fat fraction and T2* mapping using compressed sensing. PLoS ONE, 2019, 14, e0224988.	2.5	12
104	Reduction of vibrationâ€induced signal loss by matching mechanical vibrational states: Application in high <i>b</i> â€value diffusionâ€weighted MRS. Magnetic Resonance in Medicine, 2020, 84, 39-51.	3.0	12
105	Trajectory correction based on the gradient impulse response function improves highâ€resolution UTE imaging of the musculoskeletal system. Magnetic Resonance in Medicine, 2021, 85, 2001-2015.	3.0	12
106	Magnetic Resonance Imaging of Adipose Tissue in Metabolic Dysfunction. RoFo Fortschritte Auf Dem Gebiet Der Rontgenstrahlen Und Der Bildgebenden Verfahren, 2018, 190, 1121-1130.	1.3	11
107	Preconditioned waterâ€fat total field inversion: Application to spine quantitative susceptibility mapping. Magnetic Resonance in Medicine, 2022, 87, 417-430.	3.0	11
108	Magnetic resonance imaging of ankle tendon pathology: benefits of additional axial short-tau inversion recovery imaging to reduce magic angle effects. Skeletal Radiology, 2013, 42, 499-510.	2.0	10

#	Article	IF	CITATIONS
109	Spatial variations in magnetic resonance-based diffusion of articular cartilage in knee osteoarthritis. Magnetic Resonance Imaging, 2015, 33, 1051-1058.	1.8	10
110	Lumbar muscle and vertebral bodies segmentation of chemical shift encoding-based water-fat MRI: the reference database MyoSegmenTUM spine. BMC Musculoskeletal Disorders, 2019, 20, 152.	1.9	10
111	T2 mapping of the distal sciatic nerve in healthy subjects and patients suffering from lumbar disc herniation with nerve compression. Magnetic Resonance Materials in Physics, Biology, and Medicine, 2020, 33, 713-724.	2.0	10
112	Assessment of vertebral fractures and edema of the thoracolumbar spine based on waterâ€fat and susceptibilityâ€weighted images derived from a single ultraâ€short echo time scan. Magnetic Resonance in Medicine, 2021, , .	3.0	10
113	Quadriceps and Hamstrings Morphology Is Related to Walking Mechanics and Knee Cartilage MRI Relaxation Times in Young Adults. Journal of Orthopaedic and Sports Physical Therapy, 2013, 43, 881-890.	3.5	9
114	Proton Density Fat-Fraction of Rotator Cuff Muscles Is Associated With Isometric Strength 10 Years After Rotator Cuff Repair: A Quantitative Magnetic Resonance Imaging Study of the Shoulder. American Journal of Sports Medicine, 2017, 45, 1990-1999.	4.2	9
115	Camera-based respiratory triggering improves the image quality of 3D magnetic resonance cholangiopancreatography. European Journal of Radiology, 2019, 120, 108675.	2.6	9
116	3D grating-based X-ray phase-contrast computed tomography for high-resolution quantitative assessment of cartilage: An experimental feasibility study with 3T MRI, 7T MRI and biomechanical correlation. PLoS ONE, 2019, 14, e0212106.	2.5	9
117	Physiological variation of the vertebral bone marrow water T2 relaxation time. NMR in Biomedicine, 2021, 34, e4439.	2.8	9
118	Quantitative Muscle MRI in Patients with Neuromuscular Diseases—Association of Muscle Proton Density Fat Fraction with Semi-Quantitative Grading of Fatty Infiltration and Muscle Strength at the Thigh Region. Diagnostics, 2021, 11, 1056.	2.6	9
119	Geometric accuracy of magnetic resonance imaging <scp>–</scp> derived virtual <scp>3â€dimensional</scp> bone surface models of the mandible in comparison to computed tomography and cone beam computed tomography <scp>:</scp> A porcine cadaver study. Clinical Implant Dentistry and Related Research, 2021, 23, 779-788.	3.7	9
120	Patellar instability MRI measurements are associated with knee joint degeneration after reconstruction of the medial patellofemoral ligament. Skeletal Radiology, 2022, 51, 535-547.	2.0	9
121	Recent Advances in Pediatric Brain, Spine, and Neuromuscular Magnetic Resonance Imaging Techniques. Pediatric Neurology, 2019, 96, 7-23.	2.1	8
122	Diffusion tensor imaging and tractography for preoperative assessment of benign peripheral nerve sheath tumors. European Journal of Radiology, 2020, 129, 109110.	2.6	8
123	Age- and BMI-related variations of fat distribution in sacral and lumbar bone marrow and their association with local muscle fat content. Scientific Reports, 2020, 10, 9686.	3.3	8
124	Age- and gender-related variations of cervical muscle composition using chemical shift encoding-based water-fat MRI. European Journal of Radiology, 2020, 125, 108904.	2.6	8
125	Texture Features of Proton Density Fat Fraction Maps from Chemical Shift Encoding-Based MRI Predict Paraspinal Muscle Strength. Diagnostics, 2021, 11, 239.	2.6	8
126	Texture Analysis Using CT and Chemical Shift Encoding-Based Water-Fat MRI Can Improve Differentiation Between Patients With and Without Osteoporotic Vertebral Fractures. Frontiers in Endocrinology, 2021, 12, 778537.	3.5	8

#	Article	IF	CITATIONS
127	High resolution reduced-FOV Diffusion Tensor Imaging of the human pons with multi-shot variable density spiral at 3T. , 2008, 2008, 5761-4.		7
128	No healing improvement after rotator cuff reconstruction augmented with an autologous periosteal flap. Knee Surgery, Sports Traumatology, Arthroscopy, 2019, 27, 3212-3221.	4.2	7
129	Regional variation of thigh muscle fat infiltration in patients with neuromuscular diseases compared to healthy controls. Quantitative Imaging in Medicine and Surgery, 2021, 11, 2610-2621.	2.0	7
130	MRI-Determined Psoas Muscle Fat Infiltration Correlates with Severity of Weight Loss during Cancer Cachexia. Cancers, 2021, 13, 4433.	3.7	7
131	Qualitative and Quantitative Comparison of Respiratory Triggered Reduced Field-of-View (FOV) Versus Full FOV Diffusion Weighted Imaging (DWI) in Pancreatic Pathologies. Academic Radiology, 2021, 28, S234-S243.	2.5	7
132	Susceptibility artifact correction in MR thermometry forÂmonitoring of mild radiofrequency hyperthermia usingÂtotal field inversion. Magnetic Resonance in Medicine, 2022, 88, 120-132.	3.0	7
133	Gradient nonlinearity correction in liver DWI using motion-compensated diffusion encoding waveforms. Magnetic Resonance Materials in Physics, Biology, and Medicine, 2021, , 1.	2.0	7
134	Estimating vertebral bone marrow fat unsaturation based on shortâ€TE STEAM MRS. Magnetic Resonance in Medicine, 2021, 85, 615-626.	3.0	6
135	Noise reduction in diffusion weighted MRI of the pancreas using an L1-regularized iterative SENSE reconstruction. Magnetic Resonance Imaging, 2022, 87, 1-6.	1.8	6
136	High-Resolution, High b-Value Computed Diffusion-Weighted Imaging Improves Detection of Pancreatic Ductal Adenocarcinoma. Cancers, 2022, 14, 470.	3.7	6
137	Multi-scanner and multi-modal lumbar vertebral body and intervertebral disc segmentation database. Scientific Data, 2022, 9, 97.	5.3	6
138	Automated assessment of paraspinal muscle fat composition based on the segmentation of chemical shift encoding-based water/fat-separated images. European Radiology Experimental, 2018, 2, 32.	3.4	5
139	Chemicalâ€ s hift encoding–based water–fat separation with multifrequency fat spectrum modeling in spinâ€lock MRI. Magnetic Resonance in Medicine, 2020, 83, 1608-1624.	3.0	5
140	Cartilage T ₂ Relaxation Times and Subchondral Trabecular Bone Parameters Predict Morphological Outcome After Matrix-Associated Autologous Chondrocyte Implantation With Autologous Bone Grafting. American Journal of Sports Medicine, 2020, 48, 3573-3585.	4.2	5
141	Regional variation in paraspinal muscle composition using chemical shift encoding-based water-fat MRI. Quantitative Imaging in Medicine and Surgery, 2020, 10, 496-507.	2.0	5
142	Association of thigh and paraspinal muscle composition in young adults using chemical shift encoding-based water‑fat MRI. Quantitative Imaging in Medicine and Surgery, 2020, 10, 128-136.	2.0	5
143	Lipid droplet–size mapping in human adipose tissue using a clinical 3T system. Magnetic Resonance in Medicine, 2021, 86, 1256-1270.	3.0	5
144	Longitudinal changes on liver proton density fat fraction differ between liver segments. Quantitative Imaging in Medicine and Surgery, 2021, 11, 1701-1709.	2.0	5

#	Article	IF	CITATIONS
145	T2 mapping of lumbosacral nerves in patients suffering from unilateral radicular pain due to degenerative disc disease. Journal of Neurosurgery: Spine, 2019, 30, 750-758.	1.7	5
146	K-space and image space combination for motion artifact correction in multicoil multishot diffusion weighted imaging. , 2008, 2008, 1675-8.		4
147	Vertebral bone marrow fat fraction changes in postmenopausal women with breast cancer receiving combined aromatase inhibitor and bisphosphonate therapy. BMC Musculoskeletal Disorders, 2019, 20, 515.	1.9	4
148	Investigation of the Relationship between MR-Based Supraclavicular Fat Fraction and Thyroid Hormones. Obesity Facts, 2020, 13, 331-343.	3.4	4
149	Patients with episodic migraine show increased T2 values of the trapezius muscles – an investigation by quantitative high-resolution magnetic resonance imaging. Cephalalgia, 2021, 41, 934-942.	3.9	4
150	Evaluation of MR-derived simulated CT-like images and simulated radiographs compared to conventional radiography in patients with shoulder pain: a proof-of-concept study. BMC Musculoskeletal Disorders, 2022, 23, 122.	1.9	4
151	CT-like MR-derived Images for the Assessment of Craniosynostosis and other Pathologies of the Pediatric Skull. Clinical Neuroradiology, 2023, 33, 57-64.	1.9	4
152	Emerging Research on Bone Health Using High-Resolution CT and MRI. Current Radiology Reports, 2014, 2, 1.	1.4	3
153	Association of Cervical and Lumbar Paraspinal Muscle Composition Using Texture Analysis of MR-Based Proton Density Fat Fraction Maps. Diagnostics, 2021, 11, 1929.	2.6	3
154	Singleâ€voxel shortâ€TR multiâ€TI multiâ€TE STEAM MRS for water–fat relaxometry. Magnetic Resonance in Medicine, 2022, 87, 2587-2599.	3.0	3
155	Velocity extraction from spin-tagging MRI images using a weighted least-squares optical flow method. , 2007, , .		2
156	Ab <i>Initio</i> Study of the Energetics of Ionic Hydration with the Polarizable Continuum Model. Nanoscale and Microscale Thermophysical Engineering, 2007, 11, 363-378.	2.6	2
157	Noninvasive in situ proton MRS in muscle tissue and bone marrow as a novel approach to identify previous freezing in a completely thawed cadaver. NMR in Biomedicine, 2020, 33, e4220.	2.8	2
158	Magnetic resonance neurography of the lumbosacral plexus at 3 Tesla – CSF-suppressed imaging with submillimeter resolution by a three-dimensional turbo spin echo sequence. Magnetic Resonance Imaging, 2020, 71, 132-139.	1.8	2
159	Association of Thigh Muscle Strength with Texture Features Based on Proton Density Fat Fraction Maps Derived from Chemical Shift Encoding-Based Water–Fat MRI. Diagnostics, 2021, 11, 302.	2.6	2
160	Association Between Adipose Tissue Proton Density Fat Fraction, Resting Metabolic Rate and FTO Genotype in Humans. Frontiers in Endocrinology, 2022, 13, 804874.	3.5	2
161	Hierarchical Multi-Resolution Graph-Cuts for Water-Fat-Silicone Separation in Breast MRI. IEEE Transactions on Medical Imaging, 2022, 41, 3253-3265.	8.9	2
162	Finite Element Analysis of Osteoporotic and Osteoblastic Vertebrae and Its Association With the Proton Density Fat Fraction From Chemical Shift Encoding-Based Water-Fat MRI – A Preliminary Study. Frontiers in Endocrinology, 0, 13, .	3.5	2

#	Article	IF	CITATIONS
163	Use of MR-based trabecular bone microstructure analysis at the distal radius for osteoporosis diagnostics: a study in post-menopausal women with breast cancer and treated with aromatase inhibitor. Clinical Cases in Mineral and Bone Metabolism, 2016, 13, 29-32.	1.0	1
164	Molecular In Vivo Imaging of Bone Marrow Adipose Tissue. Current Molecular Biology Reports, 2018, 4, 25-33.	1.6	1
165	Proton-Density Fat Fraction of Rotator Cuff Muscles Is Associated with Isometric Strength 10 Years after Rotator Cuff Repair: A Quantitative MR Imaging Study of the Shoulder. Seminars in Musculoskeletal Radiology, 2017, 21, S1-S5.	0.7	1
166	Applications of Fat Mapping. Advances in Magnetic Resonance Technology and Applications, 2020, 1, 735-777.	0.1	1
167	Postmenopausal Chinese-Singaporean Women Have a Higher Ratio of Visceral to Subcutaneous Adipose Tissue Volume than Caucasian Women of the Same Age and BMI. Diagnostics, 2021, 11, 2127.	2.6	1
168	On quantification errors of R2*\$\$ {R}_2^{ast } \$\$ and proton density fat fraction mapping in trabecularized bone marrow in the static dephasing regime. Magnetic Resonance in Medicine, 2022, 88, 1126-1139.	3.0	1
169	Ab Initio Investigation of Ionic Hydration With the Polarizable Continuum Model. , 2005, , 473.		0
170	MR-based trabecular bone microstructure is not altered in subjects with indolent systemic mastocytosis. Clinical Imaging, 2015, 39, 886-889.	1.5	0
171	Protein supplementation during 6 mo weight loss enhances body composition changes in older women. FASEB Journal, 2010, 24, 93.7.	0.5	0
172	Association of quadriceps muscle, gluteal muscle, and femoral bone marrow composition using chemical shift encoding-based water-fat MRI: a preliminary study in healthy young volunteers. European Radiology Experimental, 2020, 4, 35.	3.4	0
173	Quantitative 3-T MRI Outcome Evaluation after Spongiosa-augmented MACI at the Knee: The Importance of Subchondral Bone Parameters. Seminars in Musculoskeletal Radiology, 2020, 24, .	0.7	0
174	Regional Variation of Thigh Muscle Composition in Healthy Controls and Patients with Myotonic Dystrophy Type 2, Limb Girdle Muscular Dystrophy Type 2A, and Pompe's Disease. , 2020, 24, .		0
175	MR-derived CT-like Images for the Assessment of Acute Vertebral Fractures and Osseous Degenerative Changes in the Thoracolumbar Spine. , 2020, 24, .		0
176	Multi-Center, Multi-Vendor Reproducibility and Calibration of MRI-Based R2* for Liver Iron Quantification. Blood, 2021, 138, 2010-2010.	1.4	0
177	Editorial for "Performance of <scp>Câ€SENSE</scp> Accelerated Rapid Liver Shear Stiffness Measurement Using Displacement Wave <scp>Polarityâ€Inversion</scp> Motion Encoding: An Evaluation Studyâ€: Journal of Magnetic Resonance Imaging, 2022, 56, 766-767.	3.4	0
178	Intraindividual difference between supraclavicular and subcutaneous proton density fat fraction is associated with cold-induced thermogenesis. Quantitative Imaging in Medicine and Surgery, 2022, 12, 2877-2890.	2.0	0